










PRECLINICAL STUDY

Full-thickness skin rejuvenation by a novel dual-length microneedle radiofrequency device: A proof-of-concept study using human skin

Ga Ram Ahn MD, PhD^{1,2}  | You Na Jang PhD¹  | So Young Lee MD²  |
 Woo Ju Kim MD, MS³  | Hye Sung Han MD, PhD⁴  | Kwang Ho Yoo MD, PhD⁴  |
 Tae Hui Bae MD, PhD³  | Jaesang Barn MD⁵ | Joon Seok MD, PhD²  |
 Beom Joon Kim MD, PhD^{1,2} 

¹Department of Medicine, Graduate School, Chung-Ang University, Seoul, South Korea

²Department of Dermatology, Chung-Ang University Hospital, Seoul, South Korea

³Department of Plastic Surgery, Chung-Ang University Gwangmyeong Hospital, Seoul, South Korea

⁴Department of Dermatology, Chung-Ang University Gwangmyeong Hospital, Seoul, South Korea

⁵Banobagi Plastic Surgery, Seoul, Korea

Correspondence

Joon Seok.

Email: seokjoon923@gmail.com

Beom Joon Kim.

Email: beomjoon74@gmail.com

Abstract

Background: A novel dual-length microneedle radiofrequency (DLMR) device has been developed to achieve full-thickness skin rejuvenation by stimulating the papillary and reticular dermis simultaneously. This device's dual-level targeting concept need to be validated on human skin, although its clinical efficacy has been demonstrated in a previous study.

Objectives: This study evaluated the dual-depth targeting capability and the ability to induce rejuvenation in each layer of vertical skin anatomy, that is, the epidermis, papillary dermis, and reticular dermis, using full-thickness human facial skin samples.

Methods: Human facial skin samples were obtained from 13 Asian patients who had facelift surgery. To validate the dual-depth targeting concept, DMLR-treated skin samples were analyzed using a digital microscope, thermal imaging, and hematoxylin and eosin (H&E) staining immediately after DMLR application. On samples stained with H&E, Masson's trichrome, and Verhoeff–Van Gieson, histological observation and morphometric analysis were performed. Total collagen assay (TCA) and quantitative real-time polymerase chain reaction (qPCR) were used to assess changes in total collagen content and mRNA expression levels of collagen types I/III and vimentin, respectively.

Results: The DMLR device successfully induced thermal stimulation in the papillary and reticular dermis. The thickness, stacks, and dermal–epidermal junction convolution of the epidermis treated with DMLR were significantly increased. Collagen bundles in the dermis treated with DMLR exhibited a notable increase in thickness, density, and horizontal alignment. Dermal collagen levels were significantly higher in the morphometric and TCA data, as well as in the qPCR data for dermal matrix proteins.

Conclusions: Our DMLR device independently and precisely targeted the papillary and reticular dermis, and it appears to be an effective modality for implementing full-thickness rejuvenation.

KEYWORDS

dual-length microneedle radiofrequency device, radiofrequency, rejuvenation

Ga Ram Ahn and You Na Jang contributed equally to this work as the first authors.

This is an open access article under the terms of the Creative Commons Attribution-NonCommercial License, which permits use, distribution and reproduction in any medium, provided the original work is properly cited and is not used for commercial purposes.

© 2023 The Authors. *Lasers in Surgery and Medicine* published by Wiley Periodicals LLC.

INTRODUCTION

Each compartment of the dermis, that is, the papillary and reticular dermis, undergoes distinct histological and mechanistic changes as humans age.^{1–4} Recent studies have advanced the understanding of the different contributions to skin aging by subpopulations of dermal fibroblasts, that is, the papillary and reticular fibroblasts.^{5–7} Each subpopulation of fibroblasts in these two layers has distinct proliferative and synthetic activities, as well as morphological and immunostaining profiles.⁵ In particular, the papillary fibroblast has higher proliferative and synthetic activity, which helps to form a stratified and differentiated epidermis with epidermal ridges. The reticular fibroblast, on the other hand, is associated with an ordered network of collagen fibers and elastin strands and has lower proliferative and synthetic activity.⁵

In light of this growing body of evidence, a novel dual-length microneedle radiofrequency (DLMR) device to stimulate both compartments of the dermis has been developed. The DLMR device utilizes microneedles of two lengths determined by the vertical dimensions of the epidermis and dermis.⁸ The longer (1000 μm) microneedles are for the reticular dermis, whereas the shorter (400 μm) ones are for the papillary dermis.

Recently, a split-face designed clinical study of 24 Asian patients investigated the clinical efficacy of this device.⁹ The study reported that lateral canthal lines, skin elasticity, wrinkles, roughness, and pore volume improved significantly after 8 weeks of treatment, with no serious adverse events. However, whether the clinical result was due to the correct implementation of the dual-level targeting concept has yet to be determined. For the missing link, the concept of the device should be validated in human skin.

Therefore, this study assessed the dual-depth targeting capability of the DLMR treatment as well as its effect on histological features of each layer of skin and dermal matrix expression using full-thickness live human facial skin samples obtained from bilateral rhytidectomy (also known as facelift surgery).

MATERIALS AND METHODS

Study device

The DLMR device DoubleTite™ (AGNES Medical Co.) was used for the study. The body of the device generates 1 MHz radiofrequency (RF) energy. The bundle of disposable microneedles on the tip of its handpiece consists of five long (1000 μm) and eight short (400 μm) microneedles.

Study design and ethics

Each pair of human skin samples, both right and left sides of the lateral cheek to the preauricular area, was obtained

from face-lifting surgery (FLS, bilateral rhytidectomy of the lateral face) of 13 Asian patients with a mean age of 56.3 ± 8.23 years (range 42–71) and Fitzpatrick skin types III and IV (Supporting Information: 1). The study was conducted in compliance with the Declaration of Helsinki and Good Clinical Practice guidelines and received ethical approval from the Ethics Committee of Chung-Ang University Gwangmyeong Hospital (No. 2301-052-002).

For the validation of the dual-depth effect of DLMR, five patients (no's. 1–5) provided a pair of skin samples from both the right and left sides without prior DLMR treatment. Refer to the following section for the validation process.

For the histological analysis and total collagen assay (TCA), another five patients (no's. 6–10) underwent an *asymmetrical* DLMR treatment 4 weeks before the surgery (Figure 1). The treatment was applied on their whole face except one area, one of the two areas that were planned to be excised during the FLS, as the negative control. As a result, one of the two excised skin samples obtained in the FLS became a negative control (untreated skin) whereas the other became a test sample (DLMR-treated skin). The prior DLMR procedure was performed one pass under local topical anesthesia. Each shot included 8 W and 100 ms RF.

For the evaluation of mRNA expression level, the skin samples were obtained from the other three patients (no's. 11–13), with the same process as in the histological analysis and TCA except that they received the DLMR treatment 3 days before the FLS.

Validation of the dual-depth effect of DLMR

A digital microscope system (AM3113T Dino-Lite Premier®; Dino-Lite Korea Co.) and a thermal imaging system (FLIR A600; Teledyne FLIR Co.) were utilized for imaging. To visualize the thermal foci, the thermal image was taken while the test device induced RF coagulation (8 W, 300 ms) on the *ex vivo* skin.

To evaluate the spatial distribution of the effects of the injection and RF coagulation in human skin, the test device was applied to the *ex vivo* specimens and the immediate tissue reaction was observed. The RF parameter was set as 8 W and 100 ms. After the application, the specimens were vertically sliced to obtain the gross magnified image. Histological analysis was also performed on the RF-coagulated sample. The tissue sections were stained with hematoxylin and eosin (H&E).

Histological analysis

For the histological analysis, the tissue samples were fixed in 10% formalin, processed, and embedded in paraffin. Five μm sections were cut and placed on glass slides. H&E staining, Masson's trichrome staining, and Verhoeff–Van Gieson staining were performed

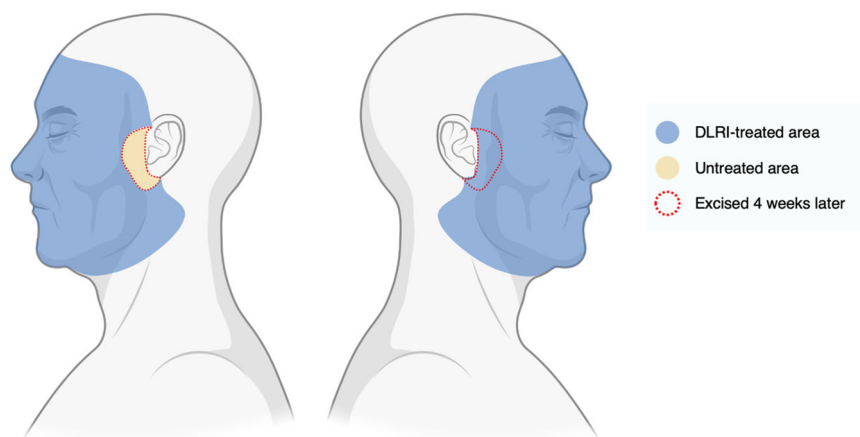


FIGURE 1 Design for human facial skin samples for evaluation of histological changes. Participants were scheduled to undergo bilateral rhytidectomy (facelift surgery) 4 weeks after receiving DLMR treatment on their full face excluding one of the preauricular regions. The DLMR treatment was administered on the full face, as indicated by the blue shading, while one of the preauricular regions was left untreated, as indicated by the yellow shading. Four weeks after DLMR treatment, both preauricular regions were excised, as indicated by the red dotted line. DLMR, dual-length microneedle radiofrequency.

under each standard protocol to evaluate general tissue morphology, collagen fibers, and elastic fibers, respectively. The images were captured using slide-imaging software (Slideviewer™; 3DHISTECH Ltd) and a digital slide scanner (PANNORAMIC™; 3DHISTECH Ltd).

An image analysis software (ImageJ; National Institutes of Health) was used for morphometric analysis. The collagen density was quantified according to previously established protocols.^{10,11} For the dermal collagen intensity, the arbitrary unit was defined as the ratio of the integrated threshold value of the sample to that of the average value in the untreated control (Supporting Information: 2). For the morphometric quantification of the epidermis, the epidermal thickness was measured at only the interrete ridge regions of the epidermis, from the basement membrane to the top of the granular layer at 10 randomly selected points across each section. The number of cell layers of the epidermis was also counted and the results were expressed as mean \pm SD according to the method of Langton et al.³ The dermal–epidermal junction (DEJ) convolution index was measured using the method of Girardeau et al.¹² (Supporting Information: 3).

TCA

Total collagen content in human skin samples was verified by using PicoSens™ total collagen assay kit (Biomax) following the manufacturer's instructions. Briefly, both DLMR-untreated and -treated sides of each sample were hydrolyzed in concentrated hydrochloric acid at 120°C for 3 h and evaporated under 70°C oven. Chloramine T reagent was added (at room temperature for 5 min), and then reacted with p-dimethylaminobenzaldehyde (DMAB) reagent (for 90 min at 60°C). Absorbance was measured at 560 nm using a microplate spectrophotometer

(SpectraMax 340; Molecular Devices, Inc.), and the results were calculated based on a standard curve generated using known concentrations of collagen type I standards included in the kit.

Quantitative polymerase chain reaction (qPCR)

Total RNA was extracted from the human skin samples using TRIzol reagent (Invitrogen). The expression levels of dermal matrix proteins were measured by fluorescence-based RT-qPCR in accordance with the MIQE précis, a practical implementation of minimum standard guidelines for fluorescence-based qPCR experiments.¹³ Single-strand cDNA synthesis from whole RNA templates was performed using Prime Script™ RT Master Mix (Takara). The primer sequence information is provided in the Supporting Information: 4. The analysis was performed using qPCR 2X PreMIX SYBR (Enzynomics) and a CFX96 Touch Real-Time PCR Detection System (Bio-Rad). The PCR amplifications were conducted under the following conditions: initial denaturation at 95°C for 10 min, followed by 30 cycles of 95°C for 10 s, 60°C for 15 s, and 72°C for 20 s. The samples were run in triplicate and normalized to a reference (glyceraldehyde 3-phosphate dehydrogenase; GAPDH). The results of the qPCR were analyzed using the $2^{-\Delta\Delta C_t}$ method to determine the relative expression levels of the target genes.

Statistics

The Student's *t*-test was used to determine significant differences between each treatment group and the untreated control (GraphPad Prism 7.0). For the *t*-test, the Shapiro–Wilk test was used to confirm whether the

sample populations were normally distributed. All numeric measurements were performed in triplicate. All data are expressed as mean \pm SD. Each mean difference was considered significant when the p -value was <0.05 .

RESULTS

Validation of the dual-length microneedles for dual-depth effect

Initially, the specifications and performance of the DLMR device (Figure 2A) were evaluated in an inorganic setting. The length of the five longer

microneedles, for the reticular dermis, was measured as $1000\ \mu\text{m}$, whereas that of the eight shorter ones, for the papillary dermis, was $400\ \mu\text{m}$ (Figure 2B,C). The thermal image of RF-discharging microneedles revealed the formation of dual-depth thermal foci (Figure 2D).

The dual-depth treatment reached each target depth, the papillary and reticular dermis in human skin (Figure 3). Clear spatial distribution of injection and coagulation effect was evident in the vertical sections of fresh samples treated with DLMR. The depth of the coagulated area on the gross section was $1025 \pm 12.8\ \mu\text{m}$ along the longer microneedles and $412.7 \pm 12.8\ \mu\text{m}$ along the shorter ones (Figure 3A). Histological analysis of DLMR-treated ex vivo human skin revealed the

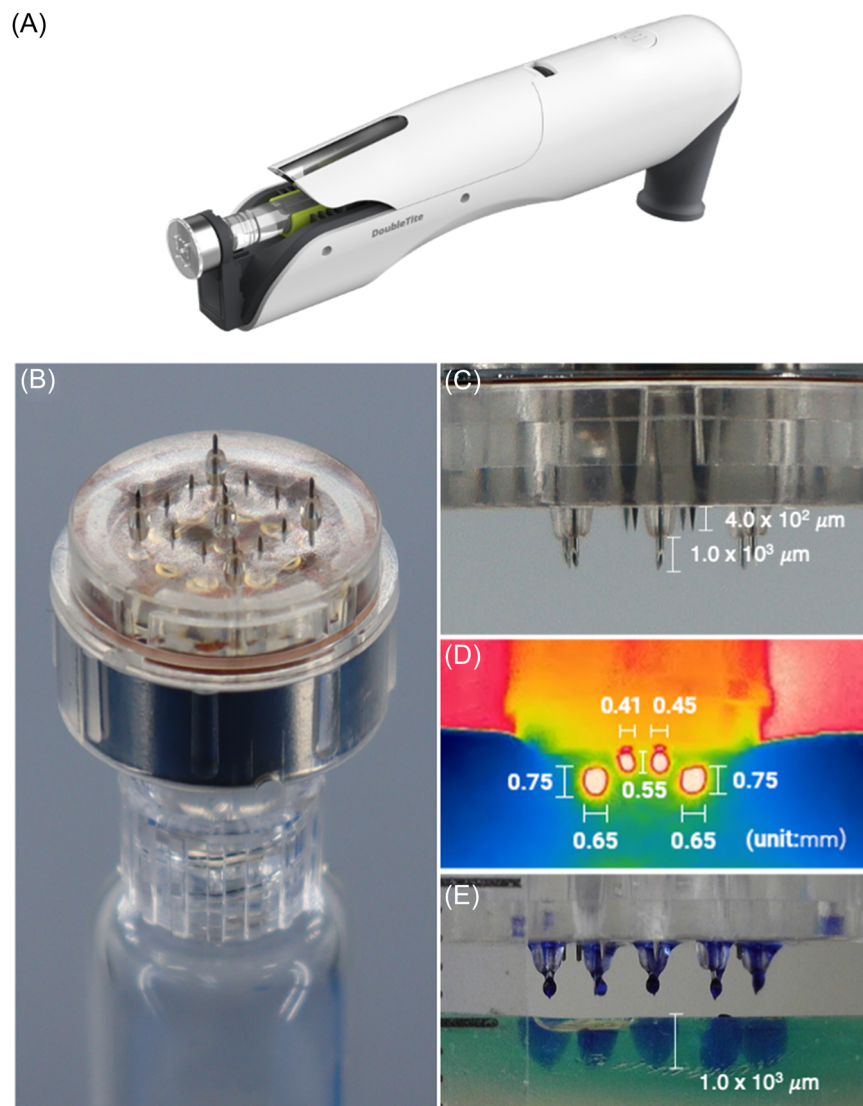


FIGURE 2 Validation of the concept of the dual-length microneedles. (A) Exterior of the handpiece (B) Oblique view of the dual-length microneedles showing its arrangement that consists of five long, hollow needles for RF and injection and eight short, solid ones for RF. (C) Side view of the microneedles. The longer ($1000\ \mu\text{m}$) microneedles are designed to target the reticular dermis whereas the shorter ($400\ \mu\text{m}$) ones are for the papillary dermis. (D) Thermal image of RF stimulation ($8\ \text{W}$, $300\ \text{ms}$). Independent dual-depth thermal foci were formed along the dual-length microneedles. (E) Injection tracks in 7% gelatin gel. The tracks were formed along the length of the longer needles. Methylene blue dye mixed with non-crosslinked hyaluronic acid (Lufila[®], Joonghun Pharmaceutical, Co., Seoul, Korea) was used for injection track visualization^{14–16} RF, radiofrequency.

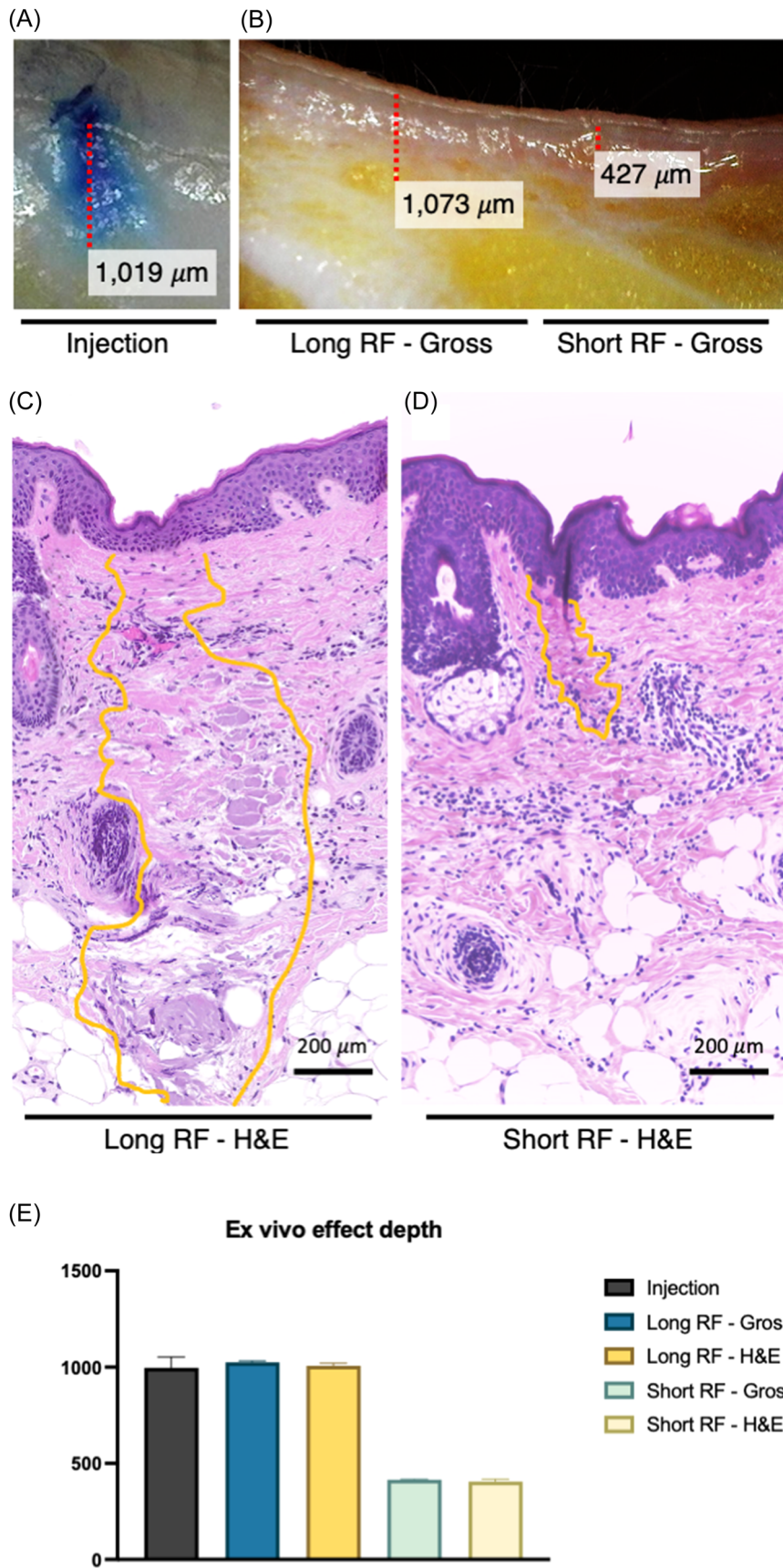


FIGURE 3 (See caption on next page).

separated dual-depth effects located at each target layer of the papillary and reticular dermis, as intended. The length of each track was 1007 ± 13.59 and $405.9 \pm 12.9 \mu\text{m}$, respectively (Figure 3B,C). Each measured length is presented in Figure 3D.

Change in quality and density of dermal matrix at weeks post-DLMR treatment

Skin samples from the DLMR-treated side of subjects who received the treatment 4 weeks before the analysis showed a marked increase in collagen bundle thickness, resulting in a decrease in interstitial spaces between these bundles, and improved alignment of the horizontal orientation of the collagen bundles as compared to that from the untreated side (Figure 4A–D). The differences in collagen density at 4 weeks post-DLMR treatment were significant in both results of morphometrical analysis (6.29%, $p < 0.0001$) and TCA (51.3%, $p < 0.0001$) (Figure 4E,F) (Table 1). The qPCR data from samples of 3 days post-DLMR treatment were consistent with the observations above (Figure 4G). The treated samples presented significantly higher mRNA expression levels of collagen type I, collagen type III, and vimentin than the untreated control (41.9%, 92.9%, and 69.1% higher, respectively).

The elastin staining revealed distinct elastin fiber characteristics on the symmetrically opposite sides of the same patient (Figure 5). The treated dermis exhibited a more prominent configuration of elastin fibers, characterized by increased thickness, improved linearity, and elongation, in comparison to the untreated region (Figure 5A,C). Especially in the treated papillary dermis, the elastin fibers coalesced into candelabra-like structures with short fibers extending perpendicular to the DEJ, whereas the untreated region displayed an absence of elastin fibers immediately below the DEJ (Figure 5B,D).

Epidermal structure change after DLMR treatment

The DLMR-treated sides exhibited notable histological characteristics of the epidermis, including increased thickness, more defined stratification, and a more convoluted DEJ as compared to the untreated ones

(Figure 6A,B). In the treated area, the keratinocytes were more organized and displayed fewer size and shape variations. In contrast, the keratinocytes in the untreated area demonstrated more characteristics of photo-aged skin,¹ including a disorganized arrangement, visible variations in size, shape, and staining properties, and prominent intracellular vacuoles that deformed the cells in the basal and spinous layers. The nuclei of these cells were frequently misshapen, peripherally deviated, and stained irregularly.

The morphometric analysis results provided quantitative evidence to support the histological observations (Figure 6C–E). Compared to the untreated area, the treated area demonstrated a 13.1% improvement in thickness ($49.6 \pm 12.1 \mu\text{m}$) as compared to the untreated area ($43.9 \pm 8.71 \mu\text{m}$) with a significant difference ($p < 0.01$) (Figure 6C). In addition, the treated area had 7.01% more live keratinocytes with nuclei per stack than the untreated side (4.27 vs. 3.99 stacks per point), a difference that was statistically significant ($p < 0.05$) (Figure 6D). The DEJ convolution index, which represents the degree of rete ridge digitation, was also 17.7% higher in the treated area than in the untreated area ($p < 0.05$; $1.32 \pm 3.15 \times 10^{-1}$ vs. $1.12 \pm 2.24 \times 10^{-1}$, respectively) (Figure 6E). A summary of the overall results of the morphometric analysis is presented in Table 1.

DISCUSSION

The data from our study demonstrated that the dual-length microneedles successfully induced distinct effects in the papillary and reticular dermis, proving the dual-depth targeting concept of the DMLR device. The lengths of the microneedles were determined based on the vertical anatomy of human skin. The reported distances between the surface and the lower margins of the epidermis and dermis are 84.0 ± 23.3 and $1076.6 \pm 225.0 \mu\text{m}$, respectively.⁸ After accounting for the safety gap, such as incomplete insertion, stratum corneum, and dermal papilla height, the actual lengths were finalized as 400 and 1000 μm . To achieve this vertical separation of the coagulation effect, RF energy had to be delivered simultaneously through needles of different lengths rather than sequentially through length-modulating needles already inserted into the skin.

FIGURE 3 Validation of dual-length microneedles. Representative cases of vertical sections of fresh samples (A) and histological samples (B and C). The coagulated tracks (A) were demonstrated at different depths for the two types of microneedles: $1025 \pm 6.86 \mu\text{m}$ for the longer (1000 μm) ones and $415.5 \pm 3.50 \mu\text{m}$ for the shorter (400 μm) ones. Histological analysis further revealed that the coagulation zones (yellow lines) by each type of microneedle were induced in the different compartments of the dermis, that is, the reticular (B) and papillary dermis (C), respectively. The longer tracks were vertically located along the reticular dermis and the shorter ones were mainly located in the papillary dermis. The length of each track was 1007 ± 13.59 and $405.9 \pm 12.9 \mu\text{m}$, respectively. Each length was measured in triplicate and presented in graph (E). The histological samples were stained with H&E. Note the scale bar for the magnification. All data are expressed as mean \pm SD. H&E, hematoxylin and eosin.

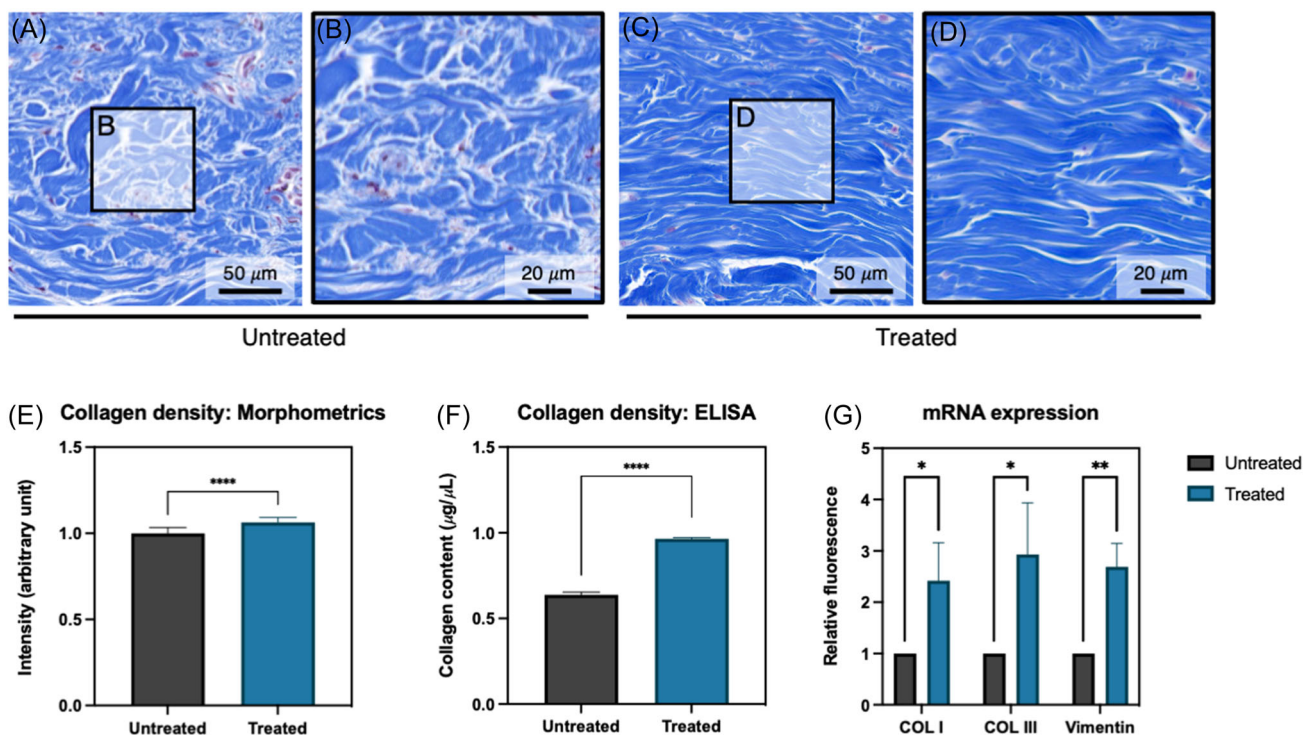


FIGURE 4 Dermal collagen changes after DLMR treatment. The representative histological samples were compared between untreated (A and B) and treated (C and D) areas. Masson's trichrome staining images of the treated area displayed denser bundles with increased thickness, reduced inter-bundle spaces, and distinct horizontal parallel alignment than that of the untreated area. These features were quantified by morphometric analysis (E) and total collagen assay (F). The collagen density significantly increased in the treated area and the differences in each analysis were 6.29% and 51.3%, respectively, 4 weeks after DLMR treatment. The mRNA expression level of collagen type I, collagen type III, and vimentin (G) also were significantly increased by 41.9%, 92.9%, and 69.1%, respectively, 3 days after the DLMR treatment. The symmetrically opposite areas of each patient were compared. Note the scale bar for the magnification. The arbitrary unit was defined as the ratio of the sample's integrated threshold value to the mean of the untreated control. (*p*-value: * <0.05 , ** <0.01 , *** <0.001 , and **** <0.0001). DLMR, dual-length microneedle radiofrequency.

TABLE 1 A summary of the overall results of the morphometric analysis and total collagen assay.

	4 weeks post-DLMR (mean \pm SD)	Untreated control (mean \pm SD)	<i>p</i> Value (95% CI)
Epidermal thickness (μ m)	49.6 \pm 12.1	43.9 \pm 8.71	4.80 $\times 10^{-3}$ (-7.06 to -4.45)
# of cell layers	4.27 \pm 9.33 $\times 10^{-1}$	3.99 \pm 8.23 $\times 10^{-1}$	1.62 $\times 10^{-2}$ (-5.06 $\times 10^{-2}$ to -5.37 $\times 10^{-2}$)
DEJ convolution index	1.32 \pm 3.15 $\times 10^{-1}$	1.12 \pm 2.24 $\times 10^{-1}$	4.69 $\times 10^{-2}$ (-3.92 $\times 10^{-1}$ to -4.42 $\times 10^{-3}$)
Collagen density (arbitrary unit)	1.10 \pm 1.06 $\times 10^{-1}$	1.00 \pm 1.16 $\times 10^{-1}$	$<1.00 \times 10^{-4}$ (-7.90 $\times 10^{-2}$ to -4.67 $\times 10^{-2}$)
Total collagen assay (μ g/ μ L)	0.965 \pm 0.478	0.638 \pm 0.480	$<1.00 \times 10^{-4}$ (2.99 $\times 10^{-1}$ to 3.55 $\times 10^{-1}$)

Abbreviations: DEJ, dermal-epidermal junction; DLMR, dual-length microneedle radiofrequency.

The previous shot in the sequential system changes the properties of the target tissue (e.g., temperature, protein structure, and water content), making it difficult to predict the effect of the subsequent RF shot.¹⁷

Our findings seem to support the clinical efficacy recently reported in a split-face clinical study by Lim et al.⁹ Their study revealed that both subjective and objective evaluations of 24 Asian participants' lateral canthus wrinkles revealed significant improvement. The quantitative measurements showed an 11.7% improvement in 3D wrinkle analysis, a 13.0% reduction in skin

roughness, and a 52.9% reduction in pore volume, which supported the clinical assessment data. These visible changes might be the result of the histological and biological effects of DLMR on human skin demonstrated in this study.

The dual-depth targeting treatment demonstrated its ability to rejuvenate multiple components and layers of human skin, as intended. The treatment enhanced the collagen fiber, a representative component of the reticular dermis, in terms of expression, quantity, density, and alignment. Elastin fibers in the papillary

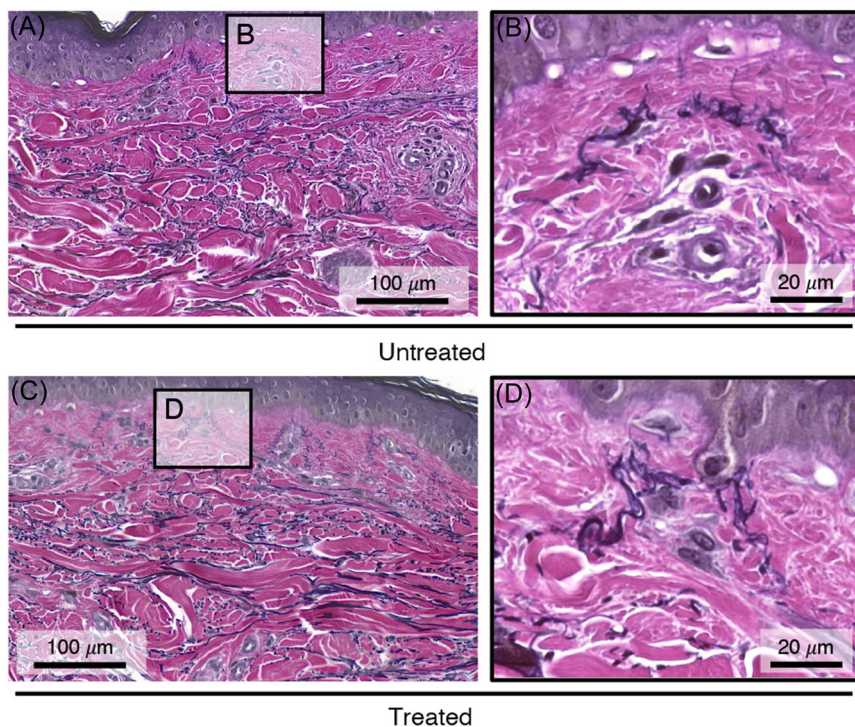


FIGURE 5 Dermal elastin changes 4 weeks post-DLMR treatment. The representative histological samples were collected 4 weeks post-DLMR treatment and compared between untreated (A and B) and treated (C and D) areas. The papillary dermis in the treated area exhibited elastin fibers coalesced into a candelabra formation with short fibers extending from the DEJ whereas the reticular dermis presented a more pronounced configuration of elastin fibers with increased thickness, improved linearity, and elongation compared to the untreated dermis. Verhoeff–Van Gieson staining was used to visualize the elastin fibers. Note the scale bar for the magnification. DEJ, dermal–epidermal junction; DLMR, dual-length microneedle radiofrequency.

dermis regained the candelabra-like structures characteristic of young, healthy skin.^{1,18} Lastly, the DLMR-treated epidermis exhibited thicker, more stacked, and more convoluted DEJ than the untreated control, consistent with previously reported literature that examined histological change after RF-induced skin rejuvenation.^{19–21}

The long-known phenomenon of dermal remodeling and rejuvenation after RF stimulation^{20–25} has recently been understood to be the clearance of stacked senescent fibroblasts, which are more heat-sensitive than younger ones.^{26,27} Accumulation of these nonfunctional but still-living fibroblasts disrupts the production of dermal matrix and the stability of the epidermal structure, resulting in the histological characteristics of aged skin. Many RF-based devices that mediate dermal heat transfer have been proposed to have a dermal rejuvenation effect by eliminating heat-sensitive senescent fibroblasts.^{28–30}

The precise separation of targets, namely the papillary and reticular dermis, is an effective strategy for the implementation of full-thickness rejuvenation. Papillary and reticular fibroblasts, subpopulations of dermal fibroblasts, have distinct contributions to the aging of the skin.^{5–7} Considering the significance of the papillary fibroblast in photo-aging, it was included as a target for

the 400 μm microneedles. Papillary fibroblasts have greater proliferative and synthetic activities than reticular fibroblasts, which validates their role in the formation of a stratified and differentiated epidermis.⁵ Mine et al. discovered that aged papillary fibroblasts have a diminished keratinopoietic effect as compared to their younger counterparts, whereas reticular fibroblasts exhibited no age-related differences.⁶ It is pertinent to the findings of Janson et al. that, after repeated sequential cultivation, papillary fibroblasts differentiate into reticular fibroblasts, which have lower synthetic activity.⁷ On the other hand, coagulating the level of the reticular dermis with the 1000 μm microneedle could not be missed. When the temperature of the reticular dermis locally exceeds 65°C, the horizontally arranged collagen bundles³¹ shrink, causing immediate skin tightening,^{32–34} and as a result, it induces remodeling of the dermal fibers by reticular fibroblasts in lower temperature surroundings.^{9,35–40} The long hollow needle of this device enables not only RF conduction but also automated intradermal drug injection with a consistent amount and depth. Although there have been previous devices that emit bipolar RF through a canular for filler injection,^{41–44} this vertically inserting multi-needle auto-injector combined with monopolar RF is a novel development. Through this needle, it is expected that a variety of substances can

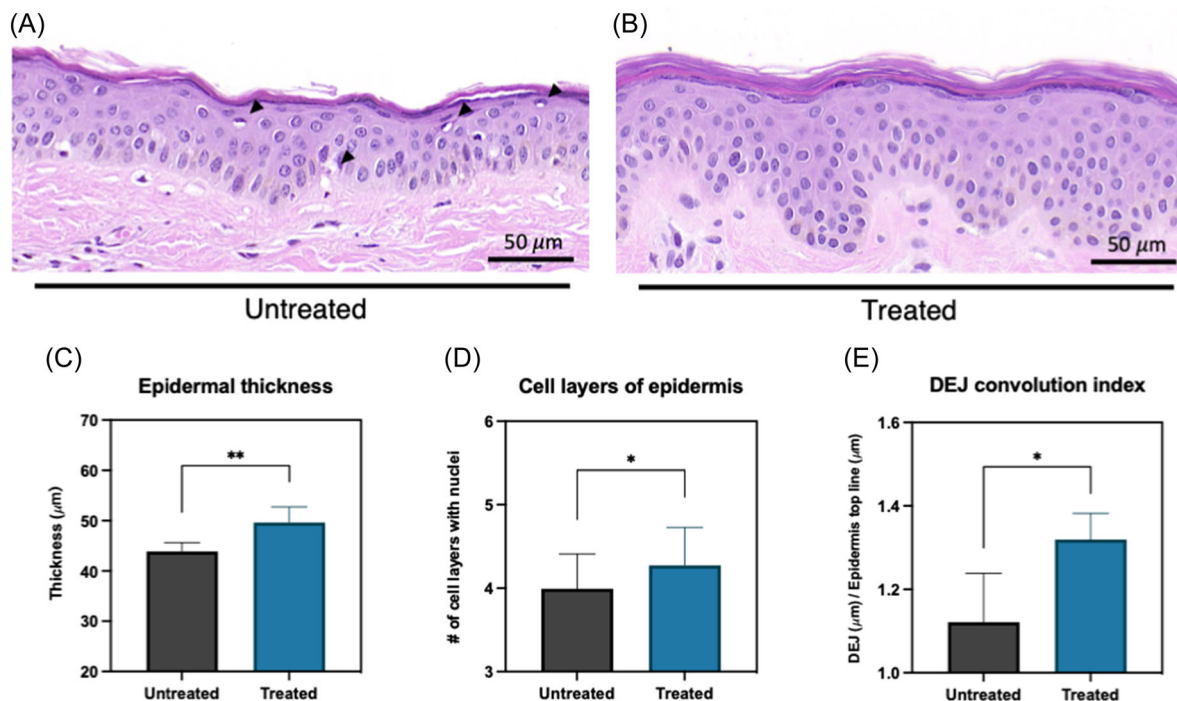


FIGURE 6 Epidermal changes after DLMR treatment. Representative histological images of the epidermis in the untreated area (A) and in the 4 weeks post-DLMR treated area (B). Both images are from symmetrically opposite sides of each patient. The epidermis in the treated area illustrated thicker and well-stratified layers and more convoluted DEJ. The untreated area often demonstrated keratinocytes heaped in disarray (size, shape, and staining properties), prominent intracellular vacuoles distorting the cells in the basal and spinous layers (arrowheads in A–C), and unrecognizable, deviated, and irregularly stained nuclei whereas the treated area did not. These features were quantified by morphometric analysis (C–E). The epidermis was 13.1% thicker (C) in the treated area as compared with the untreated area (43.9 vs. 49.6 µm). The treated side presented with 7.01% more stacks of live keratinocytes with nuclei (D) than the untreated side (3.99 vs. 4.27 per point). The DEJ convolution index was 17.7% higher (E) in the treated area than in the untreated area (1.12 vs. 1.32). The symmetrically opposite side of each subject was compared. The slides were stained with H&E. Note the scale bar for the magnification. (*p*-value: * <0.05 , ** <0.01 , *** <0.001 , and **** <0.0001). DEJ, dermal–epidermal junction; DLMR, dual-length microneedle radiofrequency; H&E, hematoxylin and eosin.

be attempted such as hyaluronic acid, poly-D,L-lactic acid,⁴⁵ and polydeoxyribonucleotide⁴⁶ to assist in the skin rejuvenation effect.

Despite these interesting results and the significance of the outcomes, our study has some limitations. The small sample size and lack of racial, age, and gender diversity may have affected the generalizability of the study's findings. In addition, the follow-up period was only 4 weeks because most patients do not schedule appointments for FLS beyond that time frame, making it difficult to design longer-term follow-up studies.

In conclusion, our findings provide evidence for the full-thickness skin rejuvenating effect of the DLMR and suggest that it is a potential modality for skin rejuvenation therapy. Further research with larger sample sizes, diversity in age, gender, ethnicity, skin types, and with longer follow-up periods is expected to confirm the efficacy and safety of the DLMR for skin rejuvenation therapy.

ACKNOWLEDGMENTS

AGNES Medical Co., (Seongnam-si, Korea) sponsored the study.

CONFLICT OF INTEREST STATEMENT

The authors declare no conflict of interest.

ORCID

Ga Ram Ahn <https://orcid.org/0000-0002-5696-4699>
 You Na Jang <https://orcid.org/0000-0002-0014-9783>
 So Young Lee <https://orcid.org/0000-0002-4119-5356>
 Woo Ju Kim <https://orcid.org/0000-0002-7817-0443>
 Hye Sung Han <http://orcid.org/0000-0002-3556-0740>
 Kwang Ho Yoo <http://orcid.org/0000-0002-0137-6849>
 Tae Hui Bae <https://orcid.org/0000-0002-0342-1439>
 Joon Seok <https://orcid.org/0000-0002-8016-8385>
 Beom Joon Kim <https://orcid.org/0000-0003-2320-7621>

REFERENCES

- Montagna W, Kirchner S, Carlisle K. Histology of sun-damaged human skin. *J Am Acad Dermatol*. 1989;21(5):907–18. [https://doi.org/10.1016/S0190-9622\(89\)70276-0](https://doi.org/10.1016/S0190-9622(89)70276-0)
- Marcos-Garcés V, Molina Aguilar P, Bea Serrano C, García Bustos V, Benavent Seguí J, Ferrández Izquierdo A, et al. Age-related dermal collagen changes during development, maturation and ageing—a morphometric and comparative study. *J Anat*. 2014;225(1):98–108. <https://doi.org/10.1111/joa.12186>

3. Langton AK, Ayer J, Griffiths TW, Rashdan E, Naidoo K, Caley MP, et al. Distinctive clinical and histological characteristics of atrophic and hypertrophic facial photoaging. *J Eur Acad Dermatol Venereol.* 2021;35(3):762–8. <https://doi.org/10.1111/jdv.17063>
4. Lynch B, Pigeon H, Le Blay H, Brizion S, Bastien P, Bornschlöggl T, et al. A mechanistic view on the aging human skin through ex vivo layer-by-layer analysis of mechanics and microstructure of facial and mammary dermis. *Sci Rep.* 2022;12(1):849. <https://doi.org/10.1038/s41598-022-04767-1>
5. Griffin MF, DesJardins-Park HE, Mascharak S, Borrelli MR, Longaker MT. Understanding the impact of fibroblast heterogeneity on skin fibrosis. *Dis Models Mech.* 2020;13(6):dmm044164. <https://doi.org/10.1242/dmm.044164>
6. Mine S, Fortunel NO, Pigeon H, Asselineau D. Aging alters functionally human dermal papillary fibroblasts but not reticular fibroblasts: a new view of skin morphogenesis and aging. *PLoS One.* 2008;3(12):e4066. <https://doi.org/10.1371/journal.pone.0004066>
7. Janson D, Saintigny G, Mahé C, Ghalbzouri AE. Papillary fibroblasts differentiate into reticular fibroblasts after prolonged in vitro culture. *Exp Dermatol.* 2013;22(1):48–53. <https://doi.org/10.1111/exd.12069>
8. Lee Y., Hwang K. Skin thickness of Korean adults. *Surg Radiol Anat.* 2002;24(3–4):183–9. <https://doi.org/10.1007/s00276-002-0034-5>
9. Lim YK, Jung CJ, Lee MY, Moon IJ, Won CH. The evaluation of efficacy and safety of a radiofrequency hydro-injector device for the skin around the eye area. *J Clin Med.* 2021;10(12):2582. <https://doi.org/10.3390/jcm10122582>
10. Chen Y, Yu Q, Xu CB. A convenient method for quantifying collagen fibers in atherosclerotic lesions by imageJ software. *Int J Clin Exp Med.* 2017;10(10):14904–10.
11. Crowe A, Yue W. Semi-quantitative determination of protein expression using immunohistochemistry staining and analysis: an integrated protocol. *Bio-Protocol.* 2019;9(24):e3465. <https://doi.org/10.21769/BioProtoc.3465>
12. Girardeau S, Mine S, Pigeon H, Asselineau D. The Caucasian and African skin types differ morphologically and functionally in their dermal component. *Exp Dermatol.* 2009;18(8):704–11. <https://doi.org/10.1111/j.1600-0625.2009.00843.x>
13. Bustin SA, Beaulieu JF, Huggett J, Jaggi R, Kibenge FS, Olsvik PA, et al. MIQE précis: practical implementation of minimum standard guidelines for fluorescence-based quantitative real-time PCR experiments. *BMC Mol Biol.* 2010;11:74. <https://doi.org/10.1186/1471-2199-11-74>
14. Jussila J. Preparing ballistic gelatine—review and proposal for a standard method. *Forensic Sci Int.* 2004;141(2–3):91–8. <https://doi.org/10.1016/j.forsciint.2003.11.036>
15. Schramm-Baxter J, Katrencik J, Mitragotri S. Jet injection into polyacrylamide gels: investigation of jet injection mechanics. *J Biomech.* 2004;37(8):1181–8. <https://doi.org/10.1016/j.jbiomech.2003.12.006>
16. Tagawa Y, Oudalov N, Ghalbzouri AE, Sun C, Lohse D. Needle-free injection into skin and soft matter with highly focused microjets. *Lab Chip.* 2013;13(7):1357. <https://doi.org/10.1039/c2lc41204g>
17. Rossmanna C, Haemmerich D. Review of temperature dependence of thermal properties, dielectric properties, and perfusion of biological tissues at hyperthermic and ablation temperatures. *Crit Rev Biomed Eng.* 2014;42(6):467–92. <https://doi.org/10.1615/critrevbiomedeng.2015012486>
18. Braverman IM, Fonferko E. Studies in cutaneous aging: I. The elastic fiber network. *J Invest Dermatol.* 1982;78(5):434–43. <https://doi.org/10.1111/1523-1747.ep12507866>
19. Timár F, Soós G, Szende B, Horváth A. Interdigitation index—a parameter for differentiating between young and older skin specimens. *Skin Res Technol.* 2000;6(1):17–20. <https://doi.org/10.1034/j.1600-0846.2000.006001017.x>
20. Sadick NS, Trelles MA. Nonablative wrinkle treatment of the face and neck using a combined diode laser and radiofrequency technology. *Dermatol Surg.* 2005;31(12):1695–9. <https://doi.org/10.2310/6350.2005.31310>
21. El-Domyati M, El-Ammawi TS, Medhat W, Moawad O, Brennan D, Mahoney G, et al. Radiofrequency facial rejuvenation: evidence-based effect. *J Am Acad Dermatol.* 2011;64(3):524–35. <https://doi.org/10.1016/j.jaad.2010.06.045>
22. Kuo T, Speyer MT, Ries WR, Reinisch L. Collagen thermal damage and collagen synthesis after cutaneous laser resurfacing. *Lasers Surg Med.* 1998;23(2):66–71. [https://doi.org/10.1002/\(SICI\)1096-9101\(1998\)23:2<66::AID-LSM3>3.0.CO;2-T](https://doi.org/10.1002/(SICI)1096-9101(1998)23:2<66::AID-LSM3>3.0.CO;2-T)
23. Liu H, Dang Y, Wang Z, Chai X, Ren Q. Laser induced collagen remodeling: a comparative study in vivo on mouse model. *Lasers Surg Med.* 2008;40(1):13–9. <https://doi.org/10.1002/lsm.20587>
24. Kelly KM, Majaron B, Nelson JS. Nonablative laser and light rejuvenation: the newest approach to photodamaged skin. *Arch Facial Plast Surg.* 2001;3(4):230–5. <https://doi.org/10.1001/archfaci.3.4.230>
25. Lolis MS, Goldberg DJ. Radiofrequency in cosmetic dermatology: a review. *Dermatol Surg.* 2012;38(11):1765–76. <https://doi.org/10.1111/j.1524-4725.2012.02547.x>
26. Cavinato M, Jansen-Dürr P. Molecular mechanisms of UVB-induced senescence of dermal fibroblasts and its relevance for photoaging of the human skin. *Exp Gerontol.* 2017;94:78–82. <https://doi.org/10.1016/j.exger.2017.01.009>
27. Fitsiou E, Pulido T, Campisi J, Alimirah F, Demaria M. Cellular senescence and the senescence-associated secretory phenotype as drivers of skin photoaging. *J Invest Dermatol.* 2021;141(4):1119–26. <https://doi.org/10.1016/j.jid.2020.09.031>
28. Yoon JE, Kim Y, Kwon S, Kim M, Kim YH, Kim JH, et al. Senescent fibroblasts drive ageing pigmentation: a potential therapeutic target for senile lentigo. *Theranostics.* 2018;8(17):4620–32. <https://doi.org/10.7150/thno.26975>
29. Kim M, Kim SM, Kwon S, Park TJ, Kang HY. Senescent fibroblasts in melasma pathophysiology. *Exp Dermatol.* 2019;28(6):719–22. <https://doi.org/10.1111/exd.13814>
30. Kwon SH, Na JI, Huh CH, Park KC. A clinical and biochemical evaluation of a temperature-controlled continuous non-invasive radiofrequency device for the treatment of melasma. *Ann Dermatol.* 2021;33(6):522. <https://doi.org/10.5021/ad.2021.33.6.522>
31. Yasui T, Tohno Y, Araki T. Characterization of collagen orientation in human dermis by two-dimensional second-harmonic-generation polarimetry. *J Biomed Opt.* 2004;9(2):259. <https://doi.org/10.1117/1.1644116>
32. Matteini P, Cicchi R, Ratto F, Kapsokalyvas D, Rossi F, de Angelis M, et al. Thermal transitions of fibrillar collagen unveiled by second-harmonic generation microscopy of corneal stroma. *Biophys J.* 2012;103(6):1179–87. <https://doi.org/10.1016/j.bpj.2012.07.055>
33. Rossmann C, Garrett-Mayer E, Rattay F, Haemmerich D. Dynamics of tissue shrinkage during ablative temperature exposures. *Physiol Meas.* 2014;35(1):55–67. <https://doi.org/10.1088/0967-3334/35/1/55>
34. Ignatieva N, Zakharkina O, Dadasheva A, Shekhter A, Sviridov A, Lunin V. Transformation of the dermal collagen framework under laser heating. *J Biophotonics.* 2019;12(12):1–10. <https://doi.org/10.1002/jbio.201960024>
35. Manstein D, Herron GS, Sink RK, Tanner H, Anderson RR. Fractional photothermolysis: a new concept for cutaneous remodeling using microscopic patterns of thermal injury. *Lasers Surg Med.* 2004;34(5):426–38. <https://doi.org/10.1002/lsm.20048>
36. Laubach HJ, Tannous Z, Anderson RR, Manstein D. Skin responses to fractional photothermolysis. *Lasers Surg Med.* 2006;38(2):142–9. <https://doi.org/10.1002/lsm.20254>
37. Rahman Z, MacFalls H, Jiang K, Chan KF, Kelly K, Tournas J, et al. Fractional deep dermal ablation induces tissue tightening.

- Lasers Surg Med. 2009;41(2):78–86. <https://doi.org/10.1002/lsm.20715>
38. No YA, Kim BJ, Kim MN, Hong CK. The clinical experience and efficacy of radiofrequency device for wrinkle treatment. *Lasers Med Sci.* 2017;32(6):1449–50. <https://doi.org/10.1007/s10103-017-2206-x>
 39. Hong JY, Kwon TR, Kim JH, Lee BC, Kim BJ. Prospective, preclinical comparison of the performance between radiofrequency microneedling and microneedling alone in reversing photoaged skin. *J Cosmet Dermatol.* 2020;19(5):1105–9. <https://doi.org/10.1111/jocd.13116>
 40. Kwon SH, Choi JY, Ahn GY, Jang WS, Shin JW, Na JI, et al. The efficacy and safety of microneedle monopolar radiofrequency for the treatment of periorbital wrinkles. *J Dermatol Treatment.* 2021;32(4):460–4. <https://doi.org/10.1080/09546634.2019.1662880>
 41. Kim H, Park KY, Choi SY, Koh HJ, Park SY, Park WS, et al. The efficacy, longevity, and safety of combined radiofrequency treatment and hyaluronic acid filler for skin rejuvenation. *Ann Dermatol.* 2014;26(4):447–56. <https://doi.org/10.5021/ad.2014.26.4.447>
 42. Ko EJ, Choi HG, Kim H, Park WS, Kim BJ, Kim MN. Novel treatment using intradermal radiofrequency and hyaluronic acid filler to correct marionette lines. *Ann Dermatol.* 2015;27(3):351–2. <https://doi.org/10.5021/ad.2015.27.3.351>
 43. Ko EJ, Kim H, Park WS, Kim BJ. Correction of midface volume deficiency using hyaluronic acid filler and intradermal radiofrequency. *J Cosmetic Laser Therapy.* 2015;17(1):46–8. <https://doi.org/10.3109/14764172.2014.968579>
 44. Hyun MY, Mun SK, Kim BJ, Kim H, Park WS. Efficacy and safety of hyaluronic acid with and without radiofrequency for forehead augmentation: a pilot study using three-dimensional imaging analysis. *Ann Dermatol.* 2016;28(1):107–9. <https://doi.org/10.5021/ad.2016.28.1.107>
 45. Hyeong JH, Jung JW, Seo SB, Kim HS, Kim KH. Intradermal injection of poly-d, l-lactic acid using microneedle fractional radiofrequency for acne scars: an open-label prospective trial. *Dermatol Surg.* 2022;48(12):1306–11. <https://doi.org/10.1097/DSS.0000000000003627>
 46. Park KY, Seok J, Rho NK, Kim BJ, Kim MN. Long-chain polynucleotide filler for skin rejuvenation: efficacy and complications in five patients. *Dermatol Ther.* 2016;29(1):37–40. <https://doi.org/10.1111/dth.12299>

SUPPORTING INFORMATION

Additional supporting information can be found online in the Supporting Information section at the end of this article.

How to cite this article: Ahn GR, Jang YN, Lee SY, Kim WJ, Han HS, Yoo KH, et al. Full-thickness skin rejuvenation by a novel dual-length microneedle radiofrequency device: a proof-of-concept study using human skin. *Lasers Surg Med.* 2023;55:758–768. <https://doi.org/10.1002/lsm.23707>